Supplement of "The grain-scale signature of isotopic diffusion in ice" by Felix S. L. Ng

Contents

S1 Matrix M in our numerical method

This section presents the elements of the matrix **M**, which we derived from Eqs. (39) and (40) by using the mixed spectral and finite difference scheme of Sect 2.6. It is convenient to partition **M** into $N \times N$ submatrices or blocks. There are five types of blocks, and we address each block's location in **M** by the column and row indices m_1 and m_2 (Fig. S1).

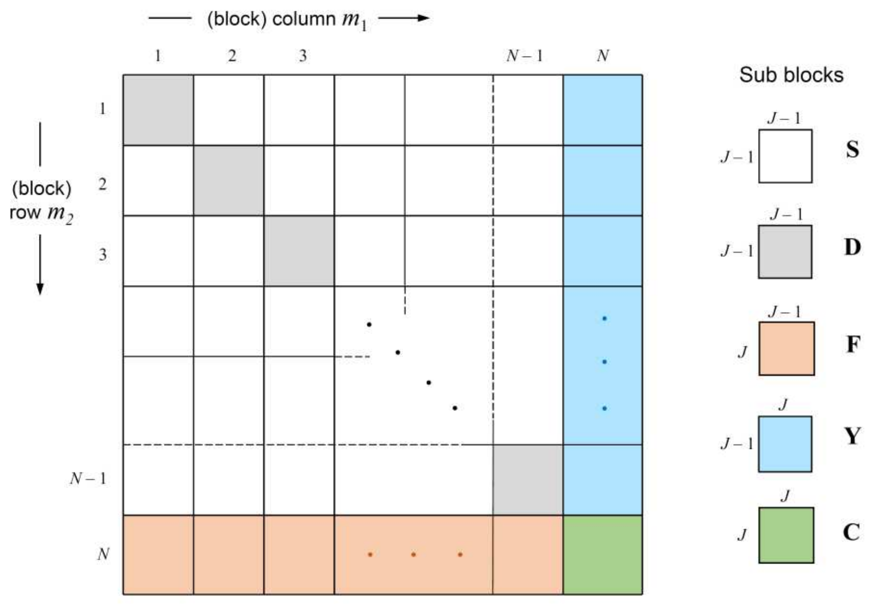

Figure S1. Structure of block matrix **M**. The key locates the five types of blocks defined in Eqs. (S3) to (S7) and indicates their sizes.

The radial step size from discretising the R-axis into J points (Fig. 3) is $\Delta = -\ln\xi / (J-1)$. Let us define the constants

$$\begin{aligned} &c_1 = -\frac{2\beta_\mathrm{b}}{\Delta^2}, \quad c_2 = \frac{\beta_\mathrm{b}}{\Delta^2} - \frac{\beta_\mathrm{b}+1}{2\Delta}, \quad c_3 = \frac{\beta_\mathrm{b}}{\Delta^2} + \frac{\beta_\mathrm{b}+1}{2\Delta}, \\ &c_4 = \frac{2(\beta_\mathrm{b}+1)}{\Delta^2}, \quad c_5 = (\beta_\mathrm{b}+1)\left(-\frac{1}{\Delta^2} + \frac{1}{2\Delta}\right), \quad c_6 = (\beta_\mathrm{b}+1)\left(-\frac{1}{\Delta^2} - \frac{1}{2\Delta}\right) \end{aligned} \tag{S1}$$

and the ingredient matrix

$$\mathbf{P} = \begin{bmatrix} e^{R_1-1} & & & \\ & e^{R_2-1} & & \\ & & \ddots & \\ & & & e^{R_{J-1}-1} \end{bmatrix}. \tag{S2}$$

Then, the blocks are given by

$$\mathbf{S}_{m_2,m_1} = -\frac{8(-1)^{N+m_1}}{\varepsilon\xi L(1+x_{m_1})}\mathbf{P}, \tag{S3}$$

$$\mathbf{D}_{m_1(=m_2)} = \mathbf{S}_{m_1,m_1} + \frac{1}{\Delta^2}\begin{bmatrix} 2e^{2(R_1-1)} & -2e^{2(R_1-1)} & & & \\ -e^{2(R_2-1)} & 2e^{2(R_2-1)} & -e^{2(R_2-1)} & & \\ & & \ddots & & \\ & & & \ddots & \\ & & -e^{2(R_{J-2}-1)} & 2e^{2(R_{J-2}-1)} & -e^{2(R_{J-2}-1)} \\ & & & -e^{2(R_{J-1}-1)} & 2e^{2(R_{J-1}-1)} \end{bmatrix}, \tag{S4}$$

$$\mathbf{F}_{m_1}(\text{rows 1 to } J-1) = -\frac{8(-1)^{N+m_1}}{\varepsilon\xi L(1+x_{m_1})}\mathbf{P}, \qquad \mathbf{F}_{m_1}(J\text{-th row}) = \begin{bmatrix} 0 & 0 & \cdots & -\frac{\pi p_2}{2\xi^2 N\Delta}\sqrt{1-{x_{m_1}}^2} \end{bmatrix}, \tag{S5}$$

$$\mathbf{Y} = \begin{bmatrix} c_1 e^{2(R_1-1)} - \beta_b k_z^2 & -c_1 e^{2(R_1-1)} & & & \\ c_2 e^{2(R_2-1)} & c_1 e^{2(R_2-1)} - \beta_b k_z^2 & c_3 e^{2(R_2-1)} & & \\ & & \ddots & & \\ & & c_2 e^{2(R_{J-2}-1)} & c_1 e^{2(R_{J-2}-1)} - \beta_b k_z^2 & c_3 e^{2(R_{J-2}-1)} \\ & & & c_2 e^{2(R_{J-1}-1)} & c_1 e^{2(R_{J-1}-1)} - \beta_b k_z^2 \quad c_3 e^{2(R_{J-1}-1)} \end{bmatrix}, \tag{S6}$$

and

$$\mathbf{C}(\text{rows 1 to } J-1) = \begin{bmatrix} c_4 e^{2(R_1-1)} + \beta_b k_z^2 & -c_4 e^{2(R_1-1)} & & & & \\ c_5 e^{2(R_2-1)} & c_4 e^{2(R_2-1)} + \beta_b k_z^2 & c_6 e^{2(R_2-1)} & & & \\ & & \ddots & & & \\ & & c_5 e^{2(R_{J-2}-1)} & c_4 e^{2(R_{J-2}-1)} + \beta_b k_z^2 & c_6 e^{2(R_{J-2}-1)} & \\ & & & c_5 e^{2(R_{J-1}-1)} & c_4 e^{2(R_{J-1}-1)} + \beta_b k_z^2 & c_6 e^{2(R_{J-1}-1)} \end{bmatrix}$$

$$\mathbf{C}(J\text{-th row}) = \begin{bmatrix} 0 & 0 & \cdots & \frac{-1}{\xi^2 \Delta}(p_2 + \frac{p_3}{L}) & p_1 + \frac{1}{\xi^2 \Delta}(p_2 + \frac{p_3}{L}) \end{bmatrix}. \qquad \text{(S7)}$$

Movie captions

Movie S1. Evolution of horizontal isotopic pattern with depth in the simulation with $T = -32$ °C, $\lambda = 2$ cm, $c = 5$ nm, $w = 0$ m yr^{-1}, and $D_b = 1.5 \times 10^{-12}$ m^2 s^{-1} (medium-high diffusivity run in Fig. 4b), compiled by sampling the normalised δ-variations in the ice annular domain at different z. (a) Depth profiles of the δ-variations at the mid-grain interior (black), grain-boundary interior (blue), and vein wall (red) over a signal wavelength. The black curve is overlain by the blue curve in this run. Dashed line marks the depth being sampled. (b) Isotopic patterns, shown with the same colour scheme as in Fig. 4. As explained in the text, although they exhibit one of two 'archetypal' forms that hardly change with depth in the corresponding stretches, their amplitude varies with depth (see colour scale) following the difference in δ between the vein and the mid-grain interior.

Movie S2. Evolution of horizontal isotopic pattern with depth in the simulation with $T = -32$ °C, $\lambda = 2$ cm, $c = 5$ nm, $w = 0$ m yr^{-1}, and $D_b = 1.5 \times 10^{-11}$ m^2 s^{-1} (high diffusivity run in Fig. 4a). The layout is the same as that in Movie S1.

Movie S3. Evolution of horizontal isotopic pattern with depth in the simulation with $T = -32$ °C, $\lambda = 2$ cm, $c = 5$ nm, $w = 0$ m yr^{-1}, and $D_b = 1.5 \times 10^{-13}$ m^2 s^{-1} (medium diffusivity run in Fig. 4c). The layout is the same as that in Movie S1.

Movie S4. Isotopic patterns from the run with $T = -32$ °C, $\lambda = 2$ cm, $c = 5$ nm, $w = 5$ m yr^{-1}, $D_b = 1.5 \times 10^{-12}$ m^2 s^{-1} (the run in Fig. 6b), compiled by sampling the solution at 55° tilt, with the tilt section meeting $z = z_2$ at $r = 0$ and the azimuth of the tilt axis varying from 0 to 360°. The patterns are shown here as they would appear when viewed along the tilt axis, instead of being reprojected onto the horizontal plane (as done in Fig. 9). The same protocol is used in Movies S5 to S7.

Movie S5. Isotopic patterns in the run with $T = -32$ °C, $\lambda = 2$ cm, $c = 5$ nm, $w = 5$ m yr^{-1}, $D_b = 1.5 \times 10^{-11}$ m^2 s^{-1} (Fig. 6a), from sampling the solution at 10° tilt, with the tilt section meeting $z = z_2$ at $r = 0$ and the tilt azimuth varying from 0 to 360°.

Movie S6. Isotopic patterns in the run with $T = -32$ °C, $\lambda = 2$ cm, $c = 5$ nm, $w = 0$ m yr^{-1}, $D_b = 1.5 \times 10^{-11}$ m^2 s^{-1} (Fig. 4a), from sampling the solution at 30° tilt, with the tilt section meeting $z = z_2$ at $r = 0$ and the tilt azimuth varying from 0 to 360°.

Movie S7. Isotopic patterns from the run with $T = -32$ °C, $\lambda = 2$ cm, $c = 5$ nm, $w = 5$ m yr^{-1}, $D_b = 1.5 \times 10^{-11}$ m^2 s^{-1} (Fig. 6a), from sampling the solution at 30° tilt, with the tilt section meeting $z = z_2$ at $r = 0$ and the tilt azimuth varying from 0 to 360°.

Figures S2–S7

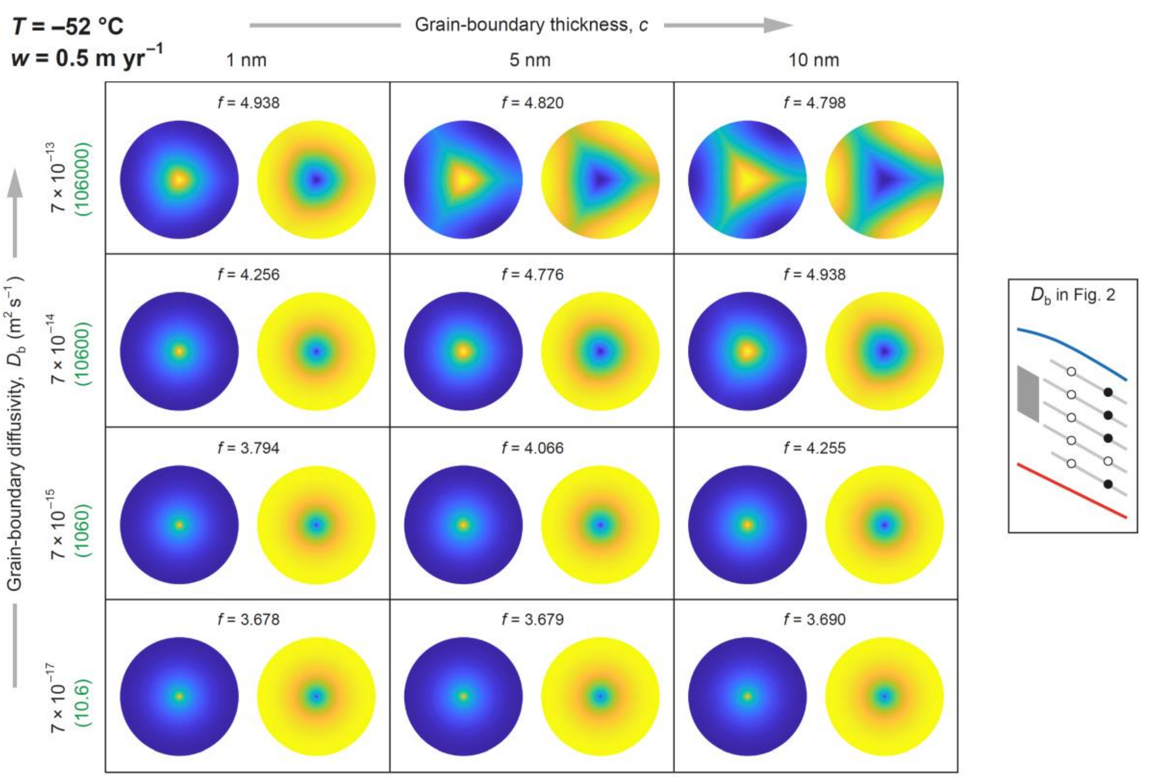

Figure S2. Dependence of archetypal patterns on grain-boundary diffusivity D_b and thickness c at –52 °C for $\lambda = 2$ cm and $w = 0.5$ m yr^{-1}. (Fig. 11 presents analogous results for $w = 0$ m yr^{-1}.) Key on the right locates the four values of D_b as black filled circles on the scheme of Fig. 2. Numbers in green give the corresponding diffusivity contrasts β_b.

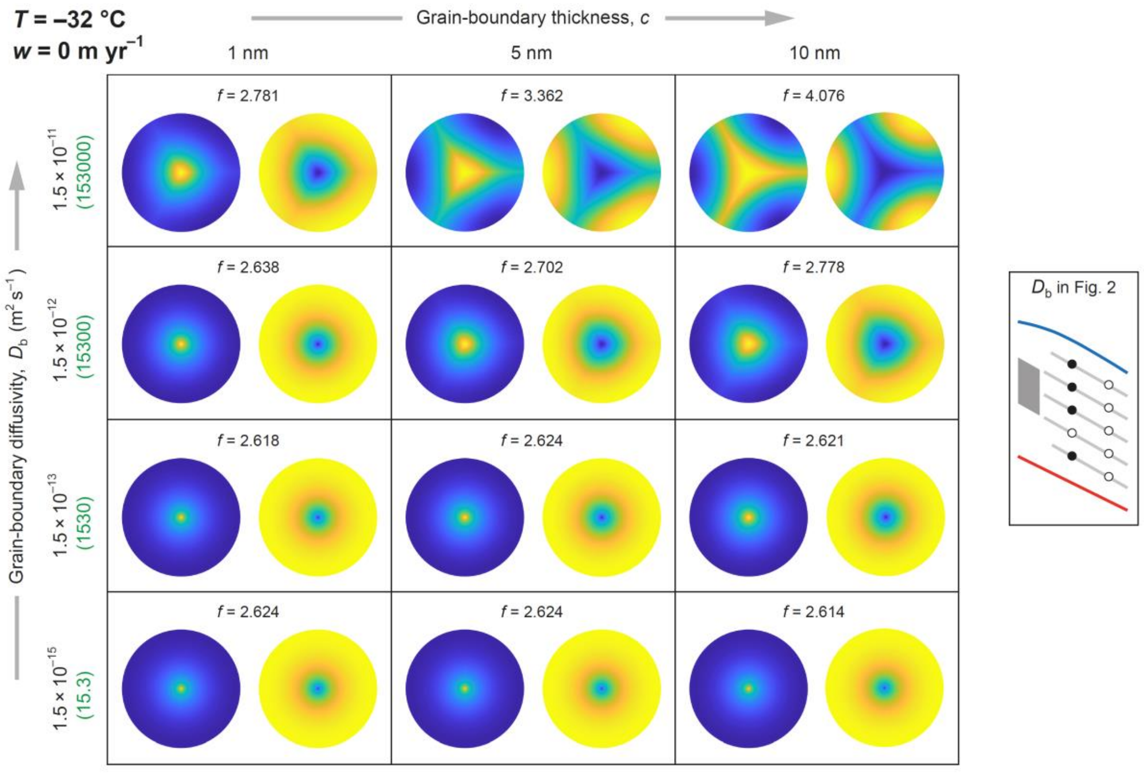

Figure S3. Dependence of archetypal patterns on D_b and c at –32 °C for λ = 8 cm and w = 0 m yr^{-1}. The key locates the values of D_b as black filled circles on the scheme of Fig. 2. Numbers in green give the corresponding diffusivity contrasts β_b.

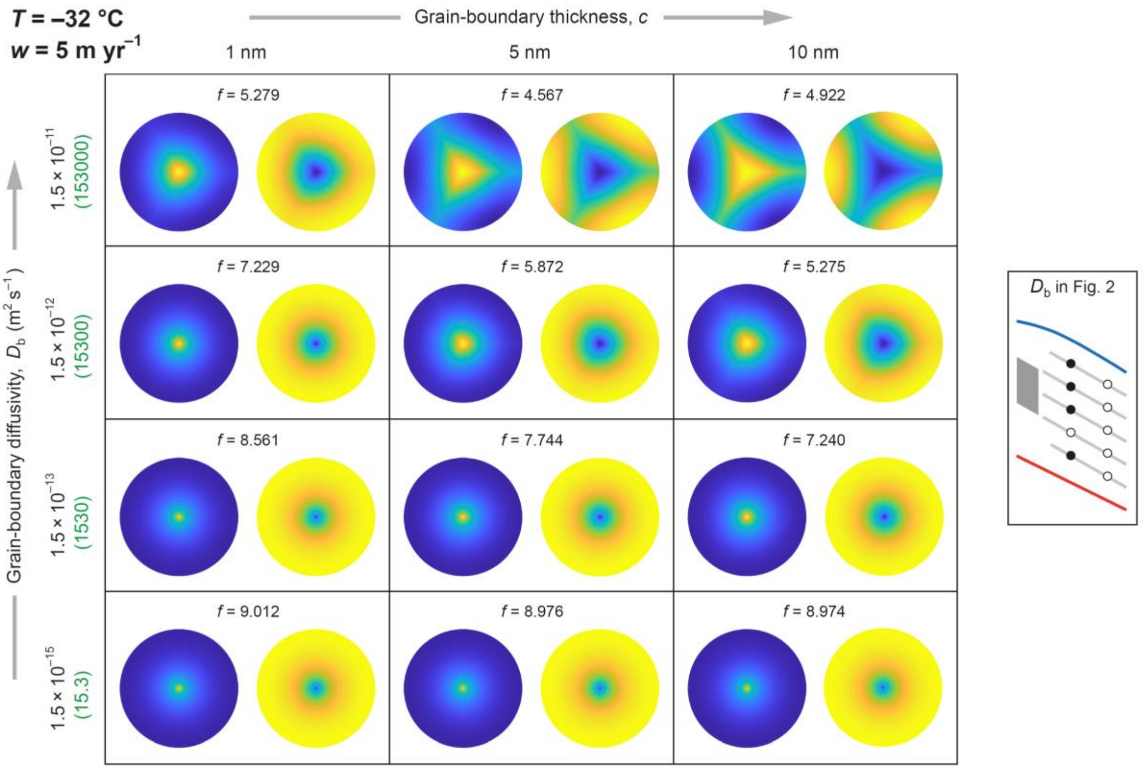

Figure S4. Dependence of archetypal patterns on D_b and c at –32 °C for $\lambda = 8$ cm and $w = 5$ m yr^{-1}. The key locates the values of D_b as black filled circles on the scheme of Fig. 2. Numbers in green give the corresponding diffusivity contrasts β_b.

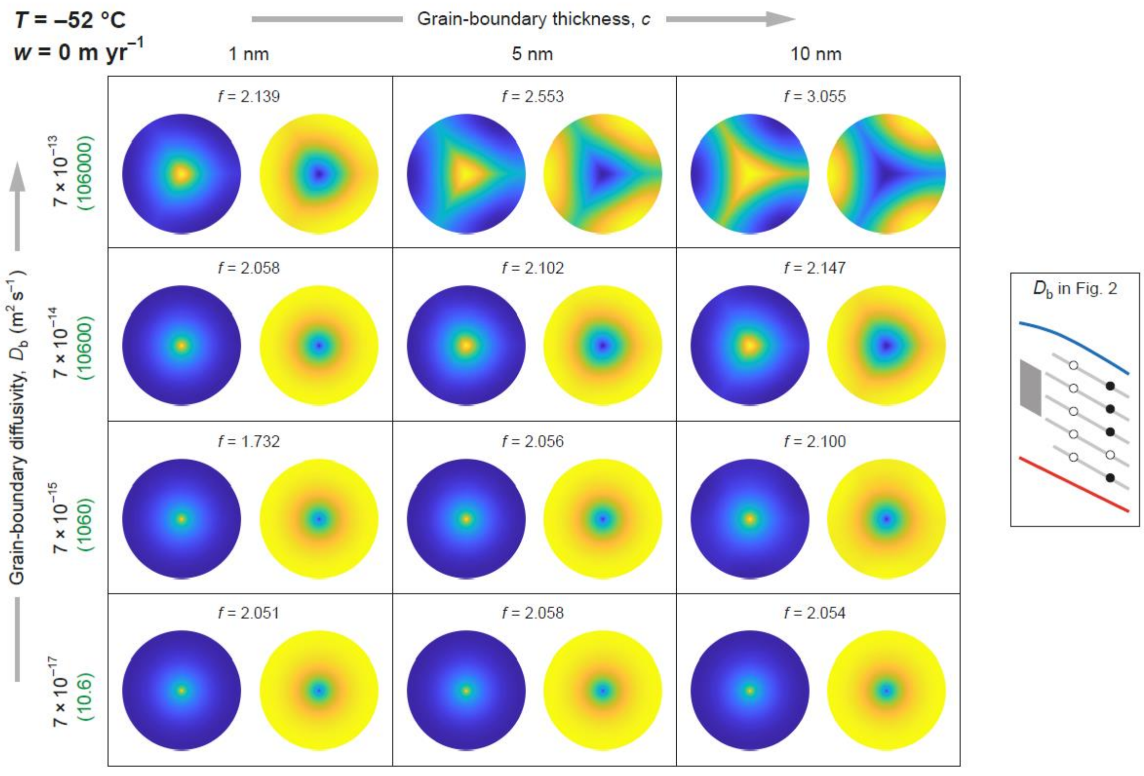

65 **Figure S5.** Dependence of archetypal patterns on D_b and c at –52 °C for $\lambda = 8$ cm and $w = 0$ m yr^{-1}. The key locates the values of D_b as black filled circles on the scheme of Fig. 2. Numbers in green give the corresponding diffusivity contrasts β_b.

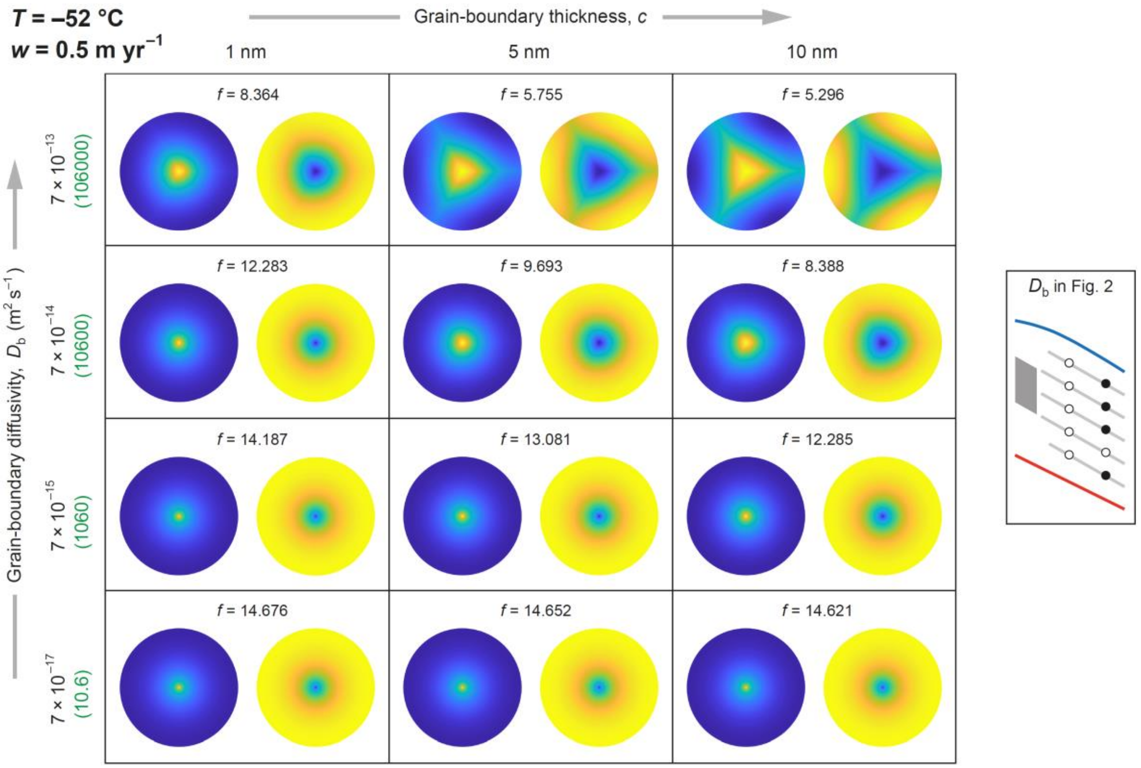

70 **Figure S6.** Dependence of archetypal patterns on D_b and c at –52 °C for λ = 8 cm and w = 0.5 m yr^{-1}. The key locates the values of D_b as black filled circles on the scheme of Fig. 2. Numbers in green give the corresponding diffusivity contrasts β_b.

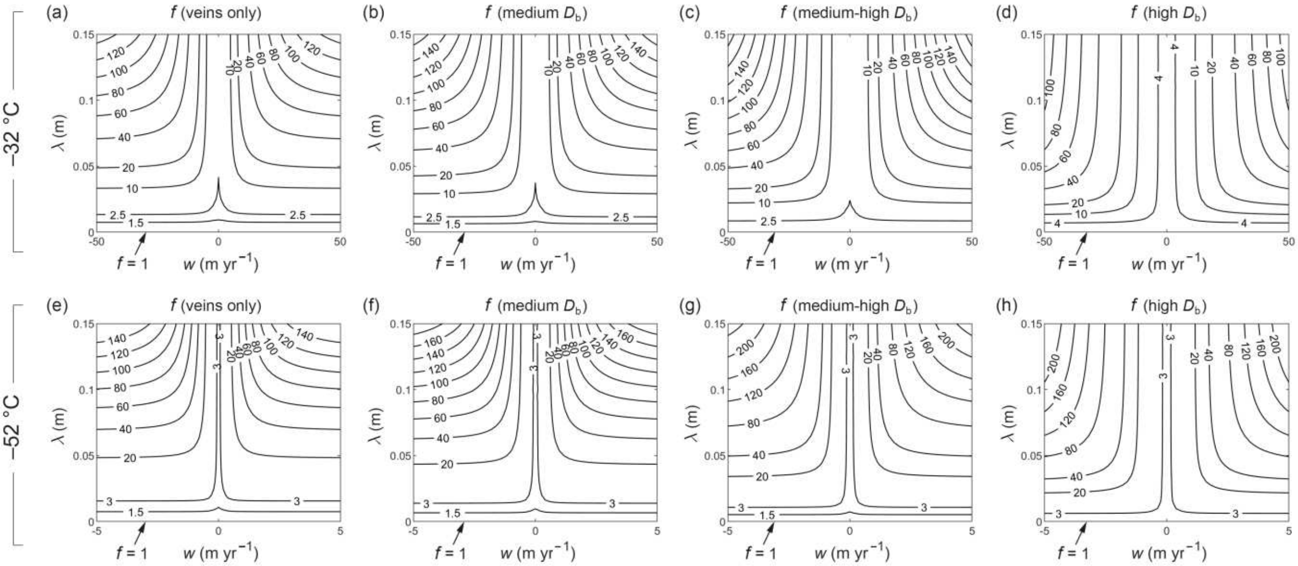

Figure S7. Impact of the presence and diffusivity (D_b) of grain boundaries on the level of excess diffusion for different vein-flow velocities w and signal wavelengths λ at –32°C and –52 °C when c = 5 nm. (a, e) Contour maps of the enhancement factor $f(w, \lambda)$ for the vein-only system without grain boundaries; data from Ng (2023). (b–d) Contour maps of f at –32 °C when D_b is medium, medium-high, and high. (f–h) Contour maps of f at –52 °C when D_b is medium, medium-high, and high.